Individual Design Task

Design of Steam Reformer using Ni-based Catalyst for Hydrogen Production

University of Bradford

Submitted by: Alexander Reeves; UoB#: 18014095
In partial fulfilment of BEng Chemical Engineering

Academic Supervisor: Professor Iqbal Mujtaba

Word count (Body): 2823

Date Submitted: 21st May 2021

ABSTRACT

The aim of the report is to produce a viable design of a steam reformer with the output capacity of 400t_{H2}/day. The overall reaction kinetics of the SR reactions are explored, and the catalyst is selected (Ni/Al_2O_3). Overall mass and energy balances confirm the throughput at feed conditions of 900^oC, 25Bar and S/C = 3.0. The total reactor volume is determined to be 54.288 m^3, with an NT of 144. Energy balances lead to specification of the required fuel feed, and a basic furnace layout is created, considering the tube layout and with a total of 54 burners.

CONTENTS

1 INTRODUCTION

Hydrogen has gained significant attention as an alternative fuel and energy source due to initiatives such as the Paris Agreement (United Nations, 2015) or the UK's 2050 net-zero goal (Committee on Climate Change, 2019). Steam Methane Reforming (SMR) produces a large amount of CO_2, efforts to reduce the emissions through methods such as Carbon Capture and Storage (CCS) have been implemented on many SMR plants within the UK (NS Energy, 2020).

What is Hydrogen used for? Hydrogen has many uses and applications within industry, for example it is used in refinery operations for Hydrotreating and Hydrocracking, as well as for metallurgical and food processing purposes (Hydrocarbon Processing, 2012).

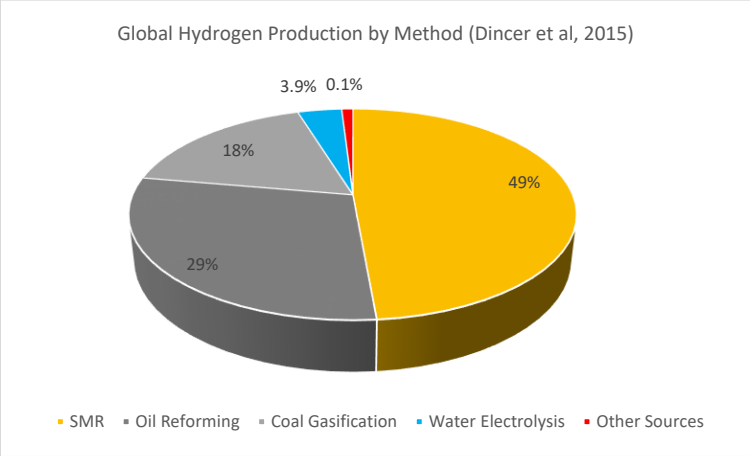

Figure 1: Global Hydrogen Production by Method (Dincer & Acar, 2015)

Globally, H_2 produced from SMR accounts for around 50% of all Hydrogen produced (Dincer & Acar, 2015). With demand projected to increase over the next decades, there is a need for design and implementation of new and optimised SMR plants. The goal of this Design Task is to produce a design of an SMR reactor with the capacity of 400t/day (H_2) using desulphurised Natural Gas as a feedstock.

Generally, SMR plants follow the process flow as displayed in *Figure 2*. This report will focus exclusively on the 'Steam Reforming' section, but the general context of the entire plant will be considered.

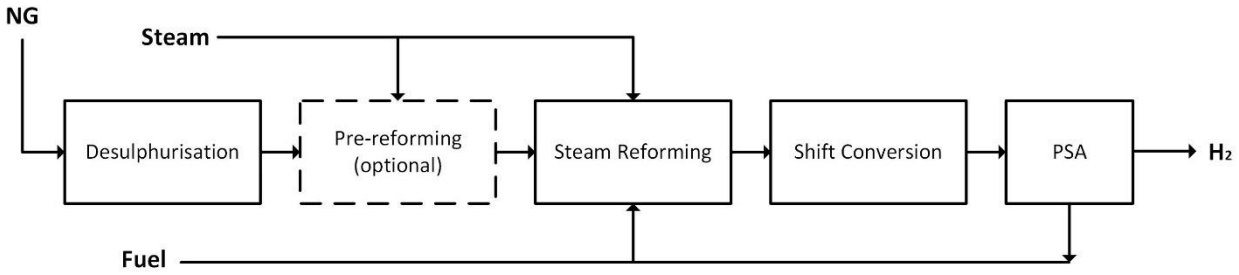

Figure 2: General SMR Plant Flow Diagram. Adapted from: Hydrocarbon Processing (2012)

As tubular reactors, also referred to as plug-flow reactors (PFR) are the main reactor type employed by the major producers of SMR plants such as Lurgi, Foster-Wheeler, Topsoe (Hydrocarbon Processing, 2012), this will be the selected reactor type.

2 METHODOLOGY

The main assumptions made for this design are listed below:

(1) Steady State Model.
(2) Isothermal and Isobaric process (ΔP calculated but not considered for mass/energy balance).
(3) Ideal radial mixing and no axial mixing within reformer tube.
(4) Gases will be considered as Ideal Gases.

2.1 Selected Feedstock

A wide variety of feedstocks are used for the SMR process, including: Natural gas, refinery off-gases, LPG, light naphta (Hydrocarbon Processing, 2012), with more advanced SR processes allowing a wider variety of feedstocks such as waste cooking oil (Pimenidou, et al., 2010).

As shown in *Figure 2*, the initial feed undergoes desulphurisation as well as pre-reforming (depending on the configuration of the plant). Based on this, the selected feedstock for the reformer was chosen as de-sulphurised Natural Gas, with Methane being the only hydrocarbon present. The composition is shown in *Table 1*. The composition was chosen to be identical to the composition used by Franchi et al., where the S/C ratio was adjusted, and the mole fractions were normalised based on that change. The S/C ratio (molar basis) was selected to be 3 (as opposed to S/C≅3.18 used by Franchi et al.), as this is a commonly used ratio for SMR (Speight, 2020) (Rosetti, 2007), and provides the necessary excess of steam required to supress carbon formation while being low enough to produce little sintering (see Section 3.5). Molar flow was decided based on the Mass Balances (Section 3.1), to achieve the throughput of 400 t_{H2}/day.

Table 1: NG Feed Composition and Flow

Feed	Mole Fraction (Franchi, et al., 2020)	Mole Fraction (This Report)	Mole Flow (kmol/h)
CH4	21.28%	22.17%	2713
CO	0.00%	0.00%	0
CO2	1.19%	1.24%	152
H2	2.6%	2.71%	332
H2O	71.45%	70.24%	8595
N2	3.49%	3.64%	445
Total	100%	100%	**12236**

2.2 Selection of Catalyst

While SR can be performed without catalyst at high temperatures, a variety of catalysts have been used for the purpose of steam reforming to increase efficiency. Nickel-based catalyst have been favoured since the initial investigations of Steam Reforming reactions (Akers & Camp, 1955), with modern research favouring Alumina-based supports such as Ni/$MgAl_2O_4$ (Xu & Froment, 1989), Ni/α-Al_2O (Hou & Hughes, 2001), and Ni/Al_2O_3 (Rashid, et al., 2017). A detailed review of many relevant Ni-based Catalysts was produced by Meloni et al. (2020).

It is common practice to impregnate a support material with the active Catalyst substance. The support material must be able to withstand high temperatures and should be chemically inert, therefore ceramics are most commonly used (Hawkins, 2013). *Figure 3* shows a range of common support shapes used for

the purpose of steam reforming (Boudreau & Rocheleau, 2010). A 4-hole catalyst support geometry was selected for the present work.

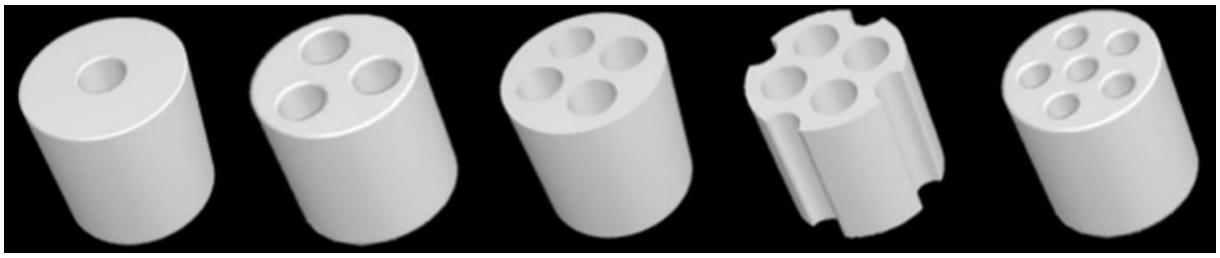

Figure 3: 1-Hole, 3-Hole, 4-Hole, 4-Hole with Grooves, 6-Hole Catalyst Support Geometries (Boudreau & Rocheleau, 2010)

A Ni/Al_2O_3 catalyst was selected for the present work, the properties are listed in *Table 3*. The data is based on the work by Rashid et al., (2017), as well as void fraction, surface area and diameter from Boudreau & Rocheleau (2010).

Table 2: Catalyst Physical Properties [1] (Rashid, et al., 2017) [2] (Boudreau & Rocheleau, 2010)

Property	Unit	Value
Density	$kg\ m^{-2}$	2719[1]
Specific Heat	$J\ kg^{-1}\ K^{-1}$	871[1]
Thermal Conductivity	$W\ m^{-1}\ K^{-1}$	202.4[1]
Catalyst Support Shape	-	4-Hole[2]
Void Fraction (porosity)	-	0.66[2]
Catalyst Diameter	m	0.025[2]
Catalyst Surface Area	m^2	0.00503[2]
Viscous Resistance	m^{-2}	6.5*10^6[1]
Internal Resistance	m^{-1}	3000[1]

The tube-do-particle diameter ratio usually lies within the range of 3-10 (Boudreau & Rocheleau, 2010). A ratio of four was chosen for this study (2.5cm catalyst diameter, 10cm diameter tubes).

Calculation of catalyst loading will be performed in section 3.3; catalyst deactivation will be discussed in the following section.

2.3 Catalyst Poisoning, Deactivation, and Replacement

There are many ways in which a catalyst can decrease in effectiveness ("de-activate"). The most commonly studied modes of deactivation are coking, poisoning, and sintering.

Coking occurs when side reactions occurring within the reformer produces coke (carbon deposits) and covers some of the catalyst area, reducing the active surface area (Meloni, et al., 2020). An excess of steam is provided to prevent this effect, though presence of steam also increases rates of sintering (Elshout, 2010).

Poisoning occurs when a contaminant (such as Sulphurs, Chlorides, As, V, Pb, Hg, or Olefins) enters the catalyst bed and reacts with the catalyst substance in a way that reduces or removes catalytic activity.

Table 3: Common Poisons - Allowable Limits (Hawkins, 2013)

Poison	Limit	Effect
Sulfur	<0.1ppmv	Poison
Chlorides	<0.1ppmv	Poison
As/V/Pb/Hg	<5ppbv	Poison
Olefins	<1-2 vol%	Carbon

It is important to keep sulphur levels low, as sulphur is commonly found within natural gas. Therefore, desulphurisation is required within H_2 plants (see *Figure 2*).

Sintering can occur when the catalyst material (metals such as Ni in the case of $NiAl_2O_3$) forms crystals on top of the support material, thereby reducing the active surface area. This effect is thermally induced usually at temperatures above 500^oC and is accelerated by presence of steam (Rosetti, 2007).

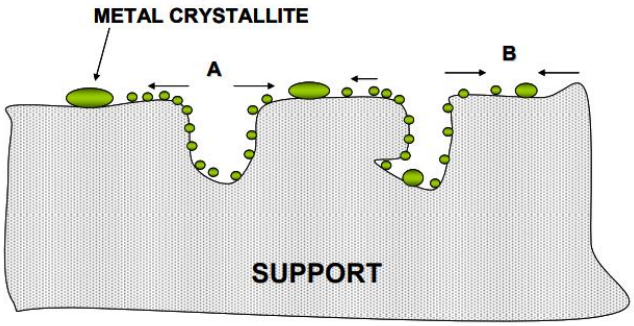

Figure 4: Two Conceptual models for crystallite growth due to sintering by (A) atomic migration or (B) crystallite migration (Rosetti, 2007)

Optimisation of the S/C ratio can be beneficial in combating these phenomena, but some amount will always be present. Predicting the exact rate of deactivation has proven difficult, with many experiments being required for more reliable predictions. Therefore, additional volume will be added to the reactor bed (Section 3.3), to provide some protection against breakthrough.

Figure 5: Different Shapes and Forms for SR Catalysts (Rosetti, 2007)

2.4 Reaction Kinetics and Activation Energy

Steam reforming reactions and kinetics have been studied in detail since the 1950s (Akers & Camp, 1955), (Xu & Froment, 1989), (Hou & Hughes, 2001).

Table 4: Equations for Steam Reforming Reaction (Hou & Hughes, 2001)

No	Reaction
1	$CH_4 + H_2O \leftrightharpoons CO + 3H_2$
2	$CO + H_2O \leftrightharpoons CO_2 + H_2$
3	$CH_4 + 2H_2O \leftrightharpoons CO_2 + 4H_2$
4	$CH_4 + CO_2 \leftrightharpoons 2CO + 2H_2$
5	$CH_4 + 3CO_2 \leftrightharpoons 4CO + 2H_2O$
6	$CH_4 \leftrightharpoons C + 2H_2$
7	$2CO \leftrightharpoons C + CO_2$
8	$CO + H_2 \leftrightharpoons C + H_2O$
9	$CO_2 + 2H_2 \leftrightharpoons C + 2H_2O$
10	$CH_4 + 2CO \leftrightharpoons 3C + 2H_2O$
11	$CH_4 + CO_2 \leftrightharpoons 2C + 2H_2O$

While the list of equations that make up the overall steam reforming reaction is extensive (*Table 4*), most models of this process utilise the primary reactions: SR (1), WGSR (2), and DSR (3).

Within the present work the following reactions will be considered:

$$(SR)\ CH_4 + H_2O \leftrightharpoons \mathrm{CO} + 3H_2 \qquad \Delta H = 206\,kJ/kmol\ at\ 25^0C \qquad \textbf{Equation 1}$$

$$(WGSR)\ CO + 2H_2O \leftrightharpoons \mathrm{CO_2} + H_2 \qquad \Delta H = -41.1\,kJ/kmol\ \ at\ 25^0C \qquad \textbf{Equation 2}$$

Rate equations have been developed by Xu and Froment, as well as by Hou and Hughes.

Table 5: Rate Equations as Derived by Xu & Froment (1989) and Hou & Hughes (2001)

	Xu & Froment, 1989	Hou & Hughes, 2001
For SR:	$r_1 = \frac{k_1}{p_{H_2}^{2.5}}\left(p_{CH_4}p_{H_2O} - \frac{p_{H_2}^3 p_{CO}}{K_1}\right)/(DEN)^2$ **Equation 3**	$r_1 = \frac{k_1(p_{CH_4}p_{H_2O}^{0.5}/p_{H_2}^{1.25})(1-(p_{CO}p_{H_2}^3/K_1\,p_{CH_4}p_{H_2O}))}{(DEN)^2}$ **Equation 7**
For WG SR:	$r_2 = \frac{k_2}{p_{H_2}}\left(p_{CO}p_{H_2O} - \frac{p_{H_2}p_{CO_2}}{K_2}\right)/(DEN)^2$ **Equation 4**	$r_2 = \frac{k_2(p_{CO}p_{H_2O}^{0.5}/p_{H_2}^{0.5})(1-(p_{CO_2}p_{H_2}/K_2 p_{CO}p_{H_2O}))}{(DEN)^2}$ **Equation 8**
For DSR:	$r_3 = \frac{k_3}{p_{H_2}^{3.5}}\left(p_{CH_4}p_{H_2O}^2 - \frac{p_{H_2}^4 p_{CO_2}}{K_3}\right)/(DEN)^2$ **Equation 5**	$r_3 = \frac{k_3(p_{CH_4}p_{H_2O}/p_{H_2}^{1.75})(1-(p_{CO_2}p_{H_2}^4/K_3\,p_{CH_4}p_{H_2O}^2))}{(DEN)^2}$ **Equation 9**
(DEN)	$DEN = 1 + K_{CO}p_{CO} + K_{H_2}p_{H_2} + K_{CH_4}p_{CH_4} + \frac{K_{H_2O}p_{H_2O}}{p_{H_2}}$ **Equation 6**	$DEN = 1 + K_{CO}p_{CO} + K_H p_H^{0.5} + \frac{K_{H_2O}p_{H_2O}}{p_{H_2}}$ **Equation 10**

As further cited works such as (Rashid, et al., 2017) and (Costamagna, et al., 2020) also make use of Xu and Froment's rate equations, this rate equation will be chosen for the present work. Where the kinetic parameters were calculated as shown by Rashid et al., see *Table 6*.

Table 6: Kinetic Parameters, T in K (Rashid, et al., 2017)

Kinetic parameters, $k_i = k_{ji} \times \exp\left(\frac{E_i}{RT}\right)$		
Reaction	k_{ji} (kmol kg^{-1} h^{-1})	E_i (kJ mol^{-1})
1	4.225×10^{15} bar$^{0.5}$	240.100
2	1.955×106 bar^{-1}	67.130
3	1.020×10^{15}bar$^{0.5}$	243.900
Equilibrium constants		
K_1	$1.198 \times 10^{13} exp\left(\frac{-26830}{T}\right)$ bar^2	
K_2	$1.767 \times 10^{-2} exp\left(\frac{4400}{T}\right)$ bar^0	
K_3	$2.117 \times 10^{11} exp\left(\frac{-22430}{T}\right)$ bar^2	
Adsorption constants, $k_i = k_{ji} \times exp\left(-\frac{\Delta H_i}{RT}\right)$		
Species (i)	k_{ji}	ΔH_i (kJ kmol^{-1})
CH_4	6.65×10^{-4} bar^{-1}	−38.280
H_2O	1.77×10^{5} bar^{0}	88.680
H_2	6.12×10^{-9} bar^{-1}	−82.900
CO	8.23×10^{-5} bar^{-1}	−70.650

Given the information from *Table 5*, all required parameters can be calculated for the operating temperature of 900°C (1173.15K):

Pre-exponential factors:

$$k_1 = 4.225 * 10^{15} bar^{0.5} * \exp\left(\frac{240.1\, kJ/mol}{8.3145 \frac{J}{mol * K} * 1173.15K}\right) = 4.33 * 10^{15} \quad \textbf{Equation 11}$$

$$k_2 = 1.995 * 106 bar^{-1} * \exp\left(\frac{67.13\, kJ/mol}{8.3145 \frac{J}{mol * K} * 1173.15K}\right) = 208.6611 \quad \textbf{Equation 12}$$

Equilibrium constants:

$$K_1 = 1.198 * 10^{13} bar^2 * \exp\left(\frac{-26830}{1173.15K}\right) = 1399.9741 \quad \textbf{Equation 13}$$

$$K_2 = 1.767 * 10^{-2} bar^0 * \exp\left(\frac{4400}{1173.15K}\right) = 0.7518 \quad \textbf{Equation 14}$$

Adsorption constants (based on Freundlich's adsorption model):

$$K_{CH_4} = 6.65 * 10^{-4} bar^{-1} * \exp\left(-\frac{-38.28\, kJ/kmol}{8.3145 \frac{J}{mol * K} * 1173.15K}\right) = 6.624 * 10^{-4}$$

$$K_{H_2O} = 1.77 * 10^5 bar^0 * \exp\left(-\frac{88.68\,kJ/kmol}{8.3145\frac{J}{mol*K} * 1173.15K}\right) = 1.786 * 10^5$$

$$K_{H_2} = 6.12 * 10^{-9} bar^{-1} * \exp\left(-\frac{-82.9\,kJ/kmol}{8.3145\frac{J}{mol*K} * 1173.15K}\right) = 6.068 * 10^{-9}$$

$$K_{H_2} = 8.23 * 10^{-5} bar^{-1} * \exp\left(-\frac{-70.65\,kJ/kmol}{8.3145\frac{J}{mol*K} * 1173.15K}\right) = 8.171 * 10^{-5}$$

Where: $R = 8.3145\frac{J}{mol*K}$ and $T = 900^0C = 1173.15K$

The final Rate- and Equilibrium constants are listed in *Table 7* below:

Table 7: Rate constant k and Equilibrium Constant K

Reaction	Rate Constant k_n	Equilibrium Constant
1	$4.33*10^{15}$	1399.9741
2	208.66	0.7518

For a given Temperature Range (500°C-1100°C) the k values were calculated and plotted as ln(k) against 1/T. Datapoint 9 was disregarded as an outlier.

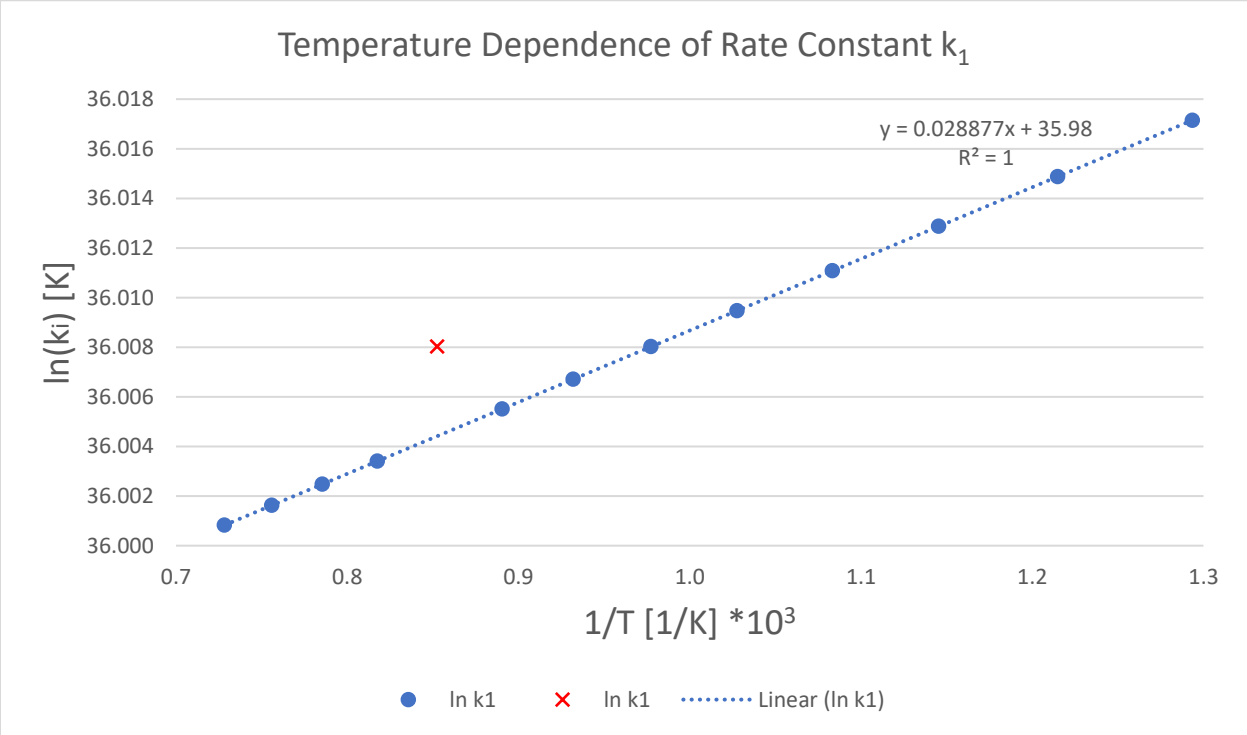

Figure 6: Temperature Dependence of Rate Constant k_1

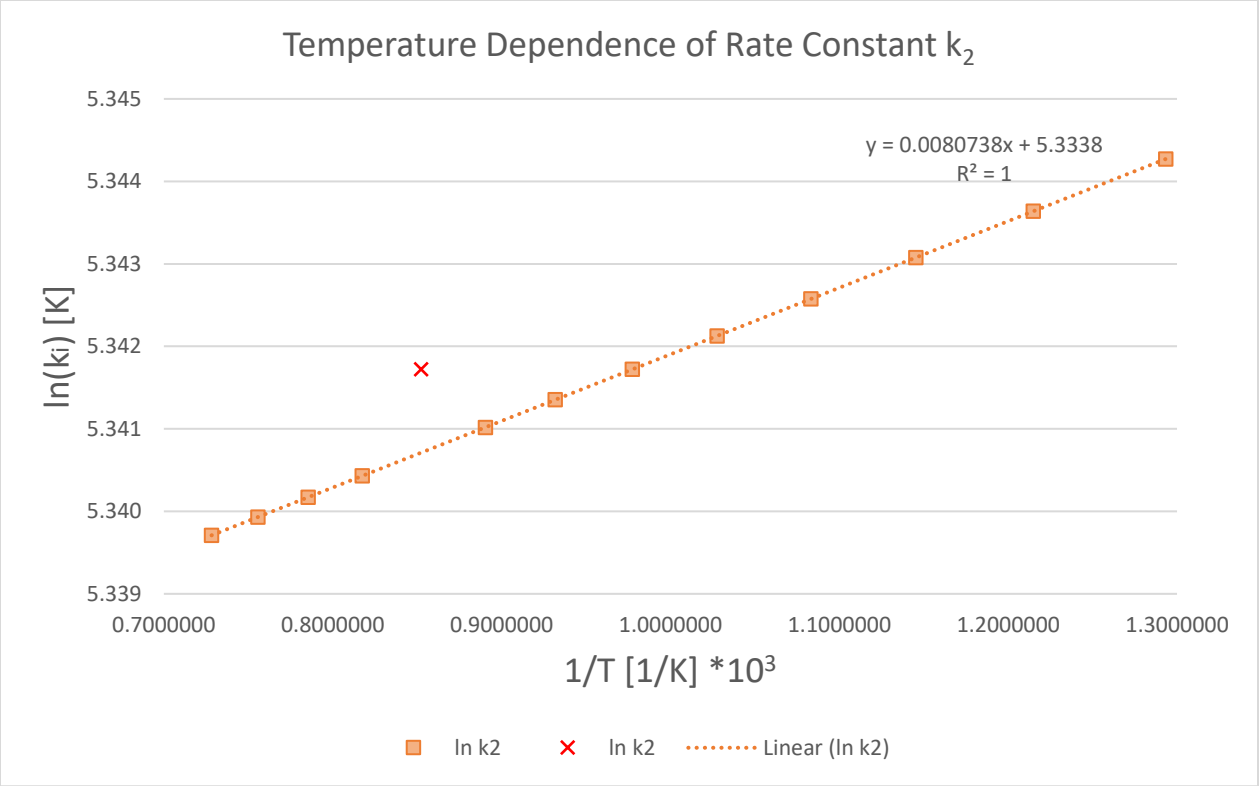

Figure 7: Temperature Dependence of Rate Constant k_2

From Figures *6* and *7* we can confirm the activation energies shown in *Table 6*, as the Arrhenius equation gives a relationship between ln(k), 1/T and activation energy E_a. This can be expressed as:

$$m\,(slope) = -E_a/R \qquad \textbf{Equation 10}$$

$$m_1 * R = -E_a \qquad \textbf{Equation 11}$$

$$-E_{a,1} = 0.028877 * 10^3 * 8.3145 = 240.1\frac{kJ}{mol}$$

$$-E_{a,2} = 0.00807381 * 10^3 * 8.3145 = 67.13\frac{kJ}{mol}$$

2.5 Thermodynamics and Equilibrium

As mentioned in Section 2.4, the SR reaction is highly endothermic (ΔH_r=206 kJ⁄kmol) and the WGSR is exothermic (ΔH_r=-41.1 kJ⁄kmol). Processes such as ATR make use of this by facilitating a reaction with no heat release or intake (ΔH_r=0), but it usually produces a lower yield compared to SMR. In the case of the SMR design, an extensive heating system must be designed to keep the reactor at a constant temperature, more on this in Section 4.

As the mass balances will be performed based on Equilibrium constants, it will be assumed that the reaction reaches equilibrium within the reactor. To achieve a mass balance, two methods of calculating equilibrium and their relationship will be utilised: Based on temperature and based on partial pressures. In Section 3.1 further explanation of the equilibrium and mass balance calculations will be given.

3 REACTOR DESIGN

3.1 Mass Balance

Mass balances were performed as an equilibrium-based species balance.

Table 8: Feed Stream Species Balance

Total Carbon (C):	2864.9	kmol
Total Oxygen (O):	8898.2	kmol
Total Hydrogen (H_2):	14352.7	kmol

Initially a species balance is performed on Carbon (C), Oxygen (O), and Hydrogen (H_2). The mole flow of CH_4 is declared as variable x, and the mole flow of CO as y. Equations can then be derived for each of the outgoing mole flows.

Carbon (C) Balance

$$2864.925 = x + y + [CO2\ out]$$
$$[CO2\ out] = 2864.925 - x - y$$ **Equation 13.1**

Oxygen (O) Balance

$$303.45 + 8594.775 + 0 = y + 2 * [CO2\ out] + [H2O\ out]$$
$$[H2O\ out] = 3168.375 + 2x + y$$ **Equation 13.2**

Hydrogen (H_2) Balance

$$5426.4 + 8594.775 + 331.5 = 2x + (3168.375 + 2x + y) + [H2\ out]$$
$$[H2\ out] = 11184.3 - 4x - y$$ **Equation 13.3**

As x and y are not known yet, sample values of 1000 for each are used, and partial pressures are defined with a total pressure of 25 Bars (2500 kPa).

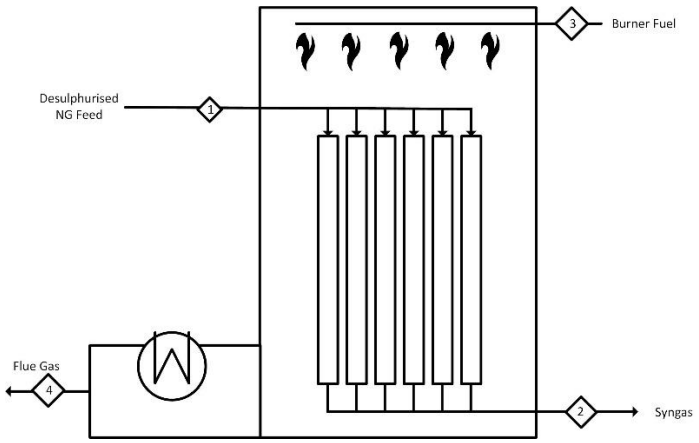

Figure 8: Process Flow Diagram

The equilibrium constants for both the SR and WGS reactions will be defined as the ratio of partial pressures according to the equation:

$$K_p = \frac{{P_C}^c * {P_D}^d}{{P_A}^a * {P_B}^b} \qquad \textbf{Equation 14.1}$$

Where the reaction is of the type: $aA + bB \rightarrow cC + dD$.

Thus, K_{reform} and K_{shift} will be defined as:

$$K_{reform} = \frac{P_{CO} * {P_{H_2}}^3}{P_{CH_4} * P_{H_2O}} \qquad \textbf{Equation 14.2}$$

$$K_{shift} = \frac{P_{CO_2} * P_{H_2}}{P_{CO} * P_{H_2O}} \qquad \textbf{Equation 14.3}$$

The equilibrium constants can also be defined from literature as dependent on temperature. This will be used to find the correct mole flows for CH_4 and CO (x and y).

$$K_{reform} = 1.198 * 10^{13} * \exp\left(\frac{-26830}{T[K]}\right) = 1.7067 * 10^{-2} * \exp\left(\frac{-26830}{1173.15K}\right) = 1399.97$$

Equation 15.1

$$K_{Shift} = 1.767 * 10^{-2} * \exp\left(\frac{4400}{T[K]}\right) = 1.7067 * 10^{-2} * \exp\left(\frac{4400}{1173.15K}\right) = 0.7518$$

Equation 15.2

Once equations 13.1 – 14.3 are confirmed, a solving algorithm (such as a Generalized Reduced Gradient (GRG) algorithm provided within Microsoft Excel) will be configured to adjust x and y to achieve the Equilibrium values obtained from equations 15.1 and 15.2. The final results are listed in *Table 9*.

Table 9: Final Mass Balance

j	y1j	n1j	Mole Flow Equations	y2j	n2j	pi (Bar)	pi (kPa)
CH4	0.222	2713	x	0.017	290	0.425	42.50
H2O	0.702	8595	3168.375 + 2x + y	0.320	5471	8.007	800.66
CO	0.000	0	y	0.101	1722	2.520	251.96
H2	0.027	332	11184.3 - 4x - y	0.486	8301	12.149	1214.92
CO2	0.012	152	2864.925 - x - y	0.050	853	1.248	124.83
N2	0.036	445	445	0.026	445	0.651	65.12
Total	**1.000**	**12236**		**1**	**17082**	**25**	**2500**

At a molar output flowrate of 8301 kmol/h (=199230 kmol/day) and using the molecular weight (2.016 kg/kmol (Perry, et al., 1997)) the final daily mass flowrate can be determined:

$$m_{out} = 199230\ kmol/day * 2.016\ kg/kmol = 401.647\ t/day \qquad \textbf{Equation 16}$$

Thus, one of the main design requirements is met.

From the final mole flow values, the reaction Extents (ξ_n), Selectivity (S), and Conversion (X_j) can be determined:

Table 10: Calculation of Extents, Selectivity, and Conversion

Extents	Selectivity	Conversion
$\xi = \frac{\Delta n_j}{a}$ **Equation 17**	$S_{j1/j2} = \frac{moles\ formed\ of\ j_1}{moles\ formed\ of\ j_2}$ **Equation 18**	$X_j = 1 - \left(\frac{n2_j}{n1_j}\right)$ **Equation 19**
$\xi_1 = \frac{2713 - 290}{-1} = 2422.73\ kmol$ $\xi_2 = 701.23\ kmol$	$S_{H_2/CO} = \frac{8284 - 332}{1722} = 4.629$	$X_{CH_4} = \frac{290}{2713} = 89.30\%$ $X_{H_2O} = \frac{5487}{8595} = 36.35\%$

3.2 Energy Balance

The energy balance is performed by the method displayed in *Figure 9*, where total energy lost due to the reaction is split into 3 terms. As the reactor will be considered isothermal, T_{in} and T_{out} will both be equal to the operating temperature, 950°C.

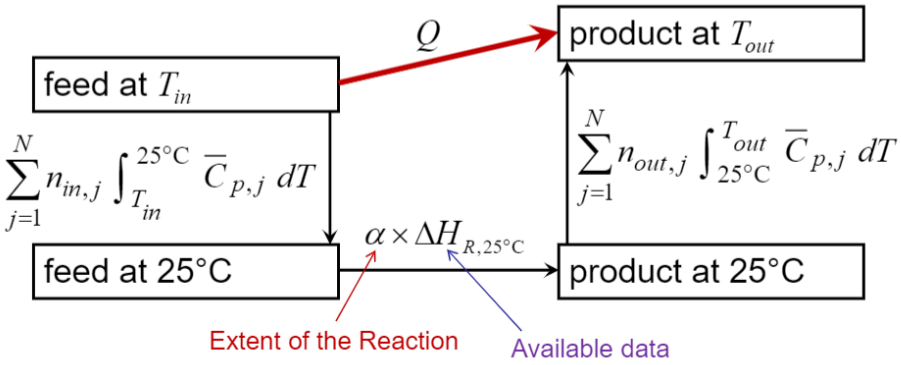

Figure 9: Method for Determining of Energy Released during Reaction (Q)

C_p values are listed in *Table 11*, where the heat capacity for any given substance takes the form: $C_{p,j} = a + bT + cT^2 + dT^3$. **Equation 20**

Table 11: Cp Parameter Table $C_{p,j} = a + bT + cT^2 + dT^3$ (Felder & Rousseau, 2005)

	a*10^3	b*10^5	c*10^8	d*10^12
CH4	19.89	0.05024	0.00001269	-1.101E-08
H2O (g)	33.46	0.688	0.7604	-3.593
CO	28.95	0.411	0.3548	-2.22
H2	28.84	0.00765	0.3288	-0.8698
CO2	22.26	0.05981	-0.00003501	7.469E-09

Term 1

The first integration is performed for T1 = 25°C and T2 = 950°C.

$$\sum_{j=1}^{N} n_{in,j} \int_{950^0C}^{25^0C} \overline{C_{p,J}}\, dT \qquad \textbf{Equation 21.1}$$

Table 11 lists the complete integration with the final value, where ΔH is calculated according to the equation:

$$\Delta \mathrm{H}_j = n_j[mol] * \left(a * (T_2 - T_1) + b * \frac{\left({T_2}^2 - {T_1}^2\right)}{2} + c * \frac{\left({T_2}^3 - {T_1}^3\right)}{3} + d * \frac{\left({T_2}^4 - {T_1}^4\right)}{4} \right) \qquad \textbf{Equation 21.2}$$

Table 12: Integration from 900°C to 25°C

	n (kmol)	T2-T1	T2^2-T1^2	T2^3-T1^3	T2^4-T1^4	ΔH
CH4	2713.2	875	809375	728984375	6.561E+11	47771572
H2O	8594.775	875	809375	728984375	6.561E+11	286379114
CO	0	875	809375	728984375	6.561E+11	0
H2	331.5	875	809375	728984375	6.561E+11	8593228
CO2	151.725	875	809375	728984375	6.561E+11	2991935
					Total (Term 1) =	**4.4051E+08 kJ**

Term 2

The second term consists of two parts. For each reaction, the extent (see mass balances) and the heats of reaction ΔH is multiplied. The resulting two values are added to give the final value for the second term.

Table 13: Heats of Reaction at 25°C

SR		***WGSR***	
ξ_1 =	2422.84 kmol	ξ_2 =	701.23
ΔH_1 =	206 kJ/kmol	ΔH_2 =	-41.1
Total =	499104.79 kJ	**Total =**	-28820.73 kJ
Term 2:	499104.79 kJ - 28820.73 kJ = **4.70E+08kJ**		

Term 3

For T1 = 950°C and T2 = 25°C.

$$\sum_{j=1}^{N} n_{out,j} \int_{25^0C}^{950^0C} \overline{C_{p,J}}\, dT \qquad \textbf{Equation 21.3}$$

Table 14: Integration from 25°C to 900°C

	n (kmol)	T2-T1	T2^2-T1^2	T2^3-T1^3	T2^4-T1^4	ΔH
CH4	290	-875	-809375	-728984375	-6.561E+11	-5112417
H2O	5471	-875	-809375	-728984375	-6.561E+11	-182284559
CO	1722	-875	-809375	-728984375	-6.561E+11	-47331257
H2	8301	-875	-809375	-728984375	-6.561E+11	-215187150
CO2	853	-875	-809375	-728984375	-6.561E+11	-16819895
					Total (Term 3):	**-4.9630E+08**

Total Q value

The final value for the total energy released (Q) follows *Equation 20.1*.

$$Q = Term\ 1 + Term\ 2 + Term\ 3$$ **Equation 22.0**

$$Q = \left(\sum_{j}^{N} n_{m,j} \int_{950^0C}^{25^0C} \overline{C_{p,J}}\, dT\right) + \left(\left(\xi_1 * \Delta \mathrm{H}_{1,25^0C}\right) + \left(\xi_2 * \Delta \mathrm{H}_{2,25^0C}\right)\right) + \left(\sum_{j}^{N} n_{m,j} \int_{25^0C}^{950^0C} \overline{C_{p,J}}\, dT\right)$$

Equation 22.1

$$Q = 4.41\mathrm{E} + (4.99\mathrm{E} + 08\ \mathrm{kJ} - 2.88\mathrm{E} + 07\ \mathrm{kJ}) - 4.96\mathrm{E} + 08\ \mathrm{kJ} = \mathbf{-1.21E + 08\ kJ}$$

The result shows a total energy requirement of **$1.21*10^8$ kJ/h**, which needs to be added to the reactor to keep the operating temperature stable (isothermal conditions).

3.3 Sizing

Initially, the tube dimensions are specified according to commonly used construction data (Piemonte & Basile, 2014).

Table 15: Tube Dimensions

Tube Length L_T	12	m
Tube Diameter $\varnothing_T$	0.1	m
Tube Thickness	0.02	m
Tube Volume V_T	0.377	m3

The sizing of the SR will be performed by integration of the rate along the conversion. The mass balances show the final conversion lies at 89.3%, therefore X_f will be equal to 0.893. The rate equation will be the same as used for the mass balance, as shown by Xu & Froment. As the rate unit is kg/m^3*s, the graph will be displayed as $M_{A0}/-r_{CH4}$.

Table 16: Reaction Rate of Methane (kg/m³*s) against Conversion

X	0	0.1	0.2	0.3	0.4	0.5	0.6	0.7	0.8	0.893
$-r_{CH4}$	30680	21585	16784	13487	10874	8592	6445	4305	2067	141
$\frac{M_{CH4,0}}{-r_{CH4}}$	1.98	2.81	3.61	4.50	5.58	7.06	9.41	14.09	29.34	430.00

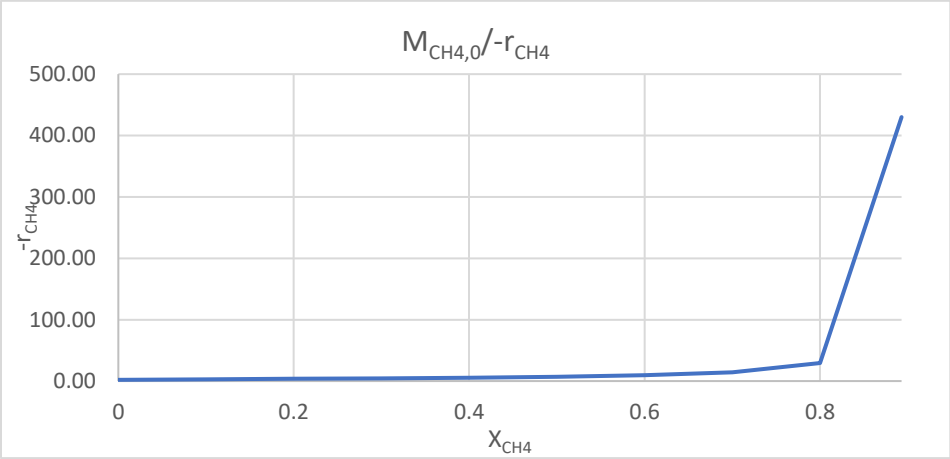

Figure 10: $M_{CH4,0}/-r_{CH4}$

Integration can be performed via the Trapezoidal method, whereby the graph is split up into trapezoids and the average areas are added together.

Table 17: Trapezoidal Integration of $M_{A0}/-r_A$

Range	b	(h1+h2)/2	b *(h1+h2)/2
0-0.1	0.1	2.392906	0.239291
0.1-0.2	0.1	3.211102	0.32111
0.2-0.3	0.1	4.054483	0.405448
0.3-0.4	0.1	5.036298	0.50363
0.4-0.5	0.1	6.317197	0.63172
0.5-0.6	0.1	8.232977	0.823298
0.6-0.7	0.1	11.74661	1.174661
0.7-0.8	0.1	21.7115	2.17115
0.8-0.893	0.1	229.6708	22.96708
Total:			29.237 m^3

The resulting volume lies at 29.237 m^3, which will be considered the total reacting volume (catalyst volume not included). The final volume (including catalyst) will be determined using the void fraction (ε = 0.66). A surplus (over-design) of 50% was also implemented, to provide a robust reactor that is able to effectively cope with higher feed rates, as well as to withstand some amount of catalyst deactivation before Hydrocarbon breakthrough occurs.

$$V_{total} = \frac{V}{\varepsilon} * 1.25 = \frac{29.237\ \mathrm{m}^3}{1 - 0.66} * 1.25 = 55.37\ m^3 \qquad \textbf{Equation 23}$$

With the tube dimensions listed in Table X, it is possible to derive the number of tubes (NT).

$$NT = \frac{V}{V_{tube}} = \frac{55.37\ m^3}{0.377\ m^3} = 146.882\ \approx 146$$ **Equation 24**

As will be discussed in Section 4: "Furnace Design", the furnace will be arranged in rows of 18 tubes. Therefore, the NT is rounded down to the nearest number divisible by 18, which is 144. This will be the final NT. Final volume is thus 144 * 0.377 m^3 = 54.288 m^3.

As mentioned, the void fraction of the catalyst is 0.66, therefore given the total reactor volume of 54.288 m^3 the volume as well as the mass of the catalyst loading can be determined (see *Table 2*):

$$V_{cat} = 54.288 * 0.66 = 35.83\ m^3$$

$$M_{cat} = \rho_{cat} * V_{cat} = 2719\ \ kg/m^3 * 35.83\ m^3 = 97421\ kg = 97.4\ t$$ **Equation 25**

The bulk density is defined as the ratio of catalyst weight to total volume.

$$\rho_b = \frac{97421\ kg}{35.83\ m^3} = 2719\ \ kg/m^3$$

The specifics of the tube layout will be discussed in Section 4 "Furnace Design".

3.4 Pressure Drop

Experimental data produced by Boudreau & Rocheleau gives a pressure drop (for 4-hole catalyst geometry) of 3176 Pa/m.

$$3176\ \ Pa/m * 12m = 38.112\ kPa = 0.38\ bar$$

3.5 Sensitivity of Temperature on Conversion, Selectivity and Rate

A sensitivity analysis was performed over a range of 500°C - 1100°. The conversion, selectivity and rate (based on rate equation by Xu & Froment) was also observed.

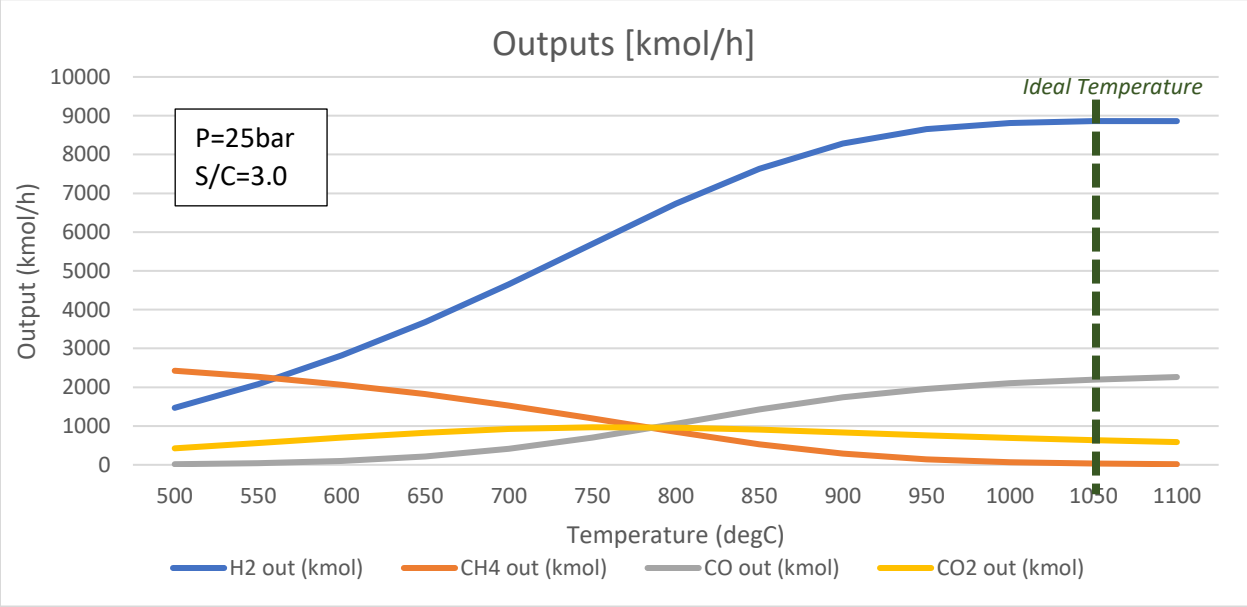

Figure 11: Sensitivity of Temperature on Outgoing Flows

The mole flow graph shows the highest output of H_2 at a temperature of 1050°C. While this would be the theoretical optimum temperature, the operating temperature of 900°C is more suited for industrial application due to lower energy consumption, and only a marginal decrease on H_2 output. It is worth noting that the CO content also increases rapidly with temperature, which will affect the shift reactors further downstream.

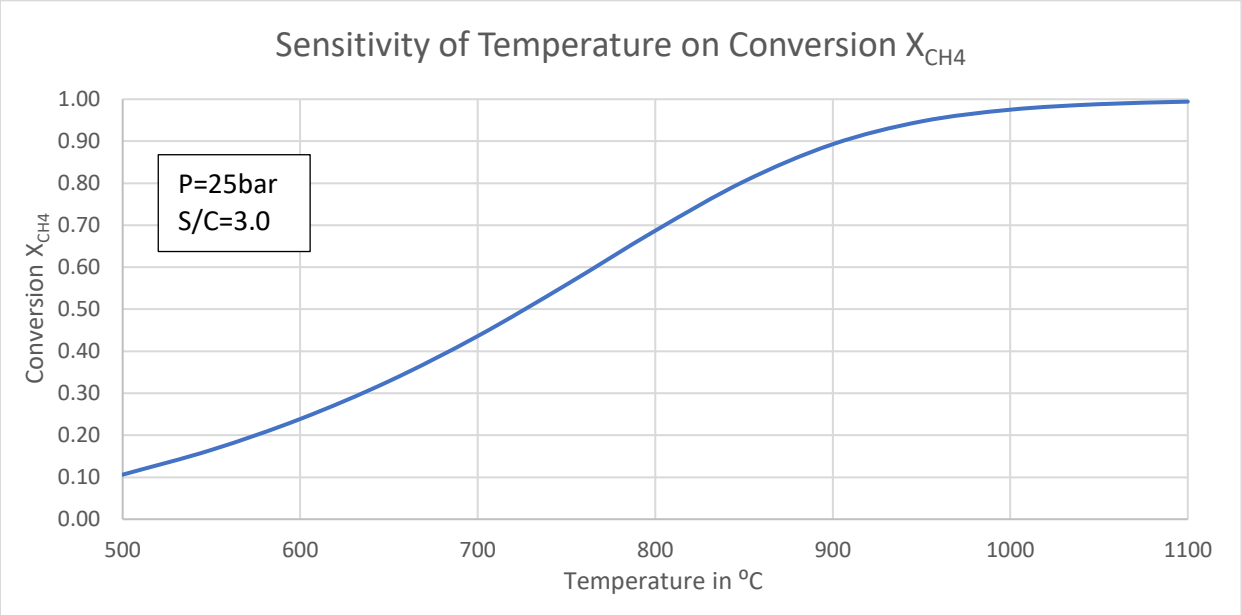

Figure 12: Sensitivity of Temperature on Conversion X_{CH4}

It can be observed that the conversion approaches 100% with increasing temperature. Once again, the conversion of 89% at an operating temperature of 900°C can be confirmed.

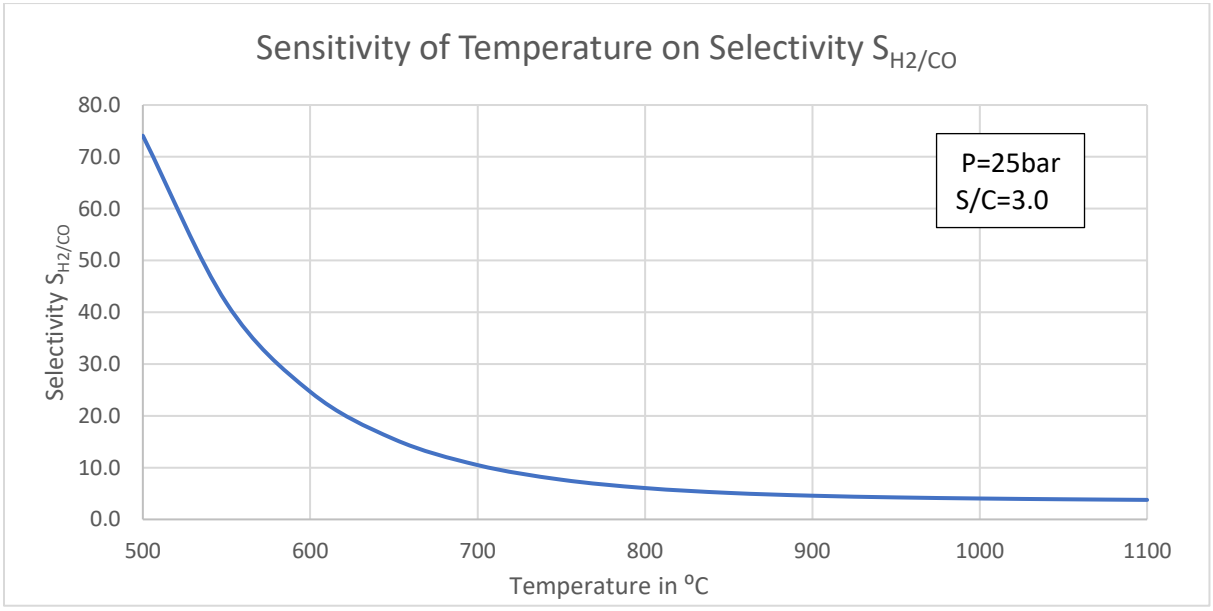

Figure 13: Sensitivity of Temperature on Selectivity $S_{H2/CO}$

Selectivity decreases sharply initially (500°C - 700°C) and levels off towards a value of 3.8 at 1100°C. At the operating temperature of 900°C the Selectivity of H_2 to CO lies at 4.6, as shown in previous calculations. The decrease shows a higher fraction of CO at higher temperatures, as shown in Figure 11.

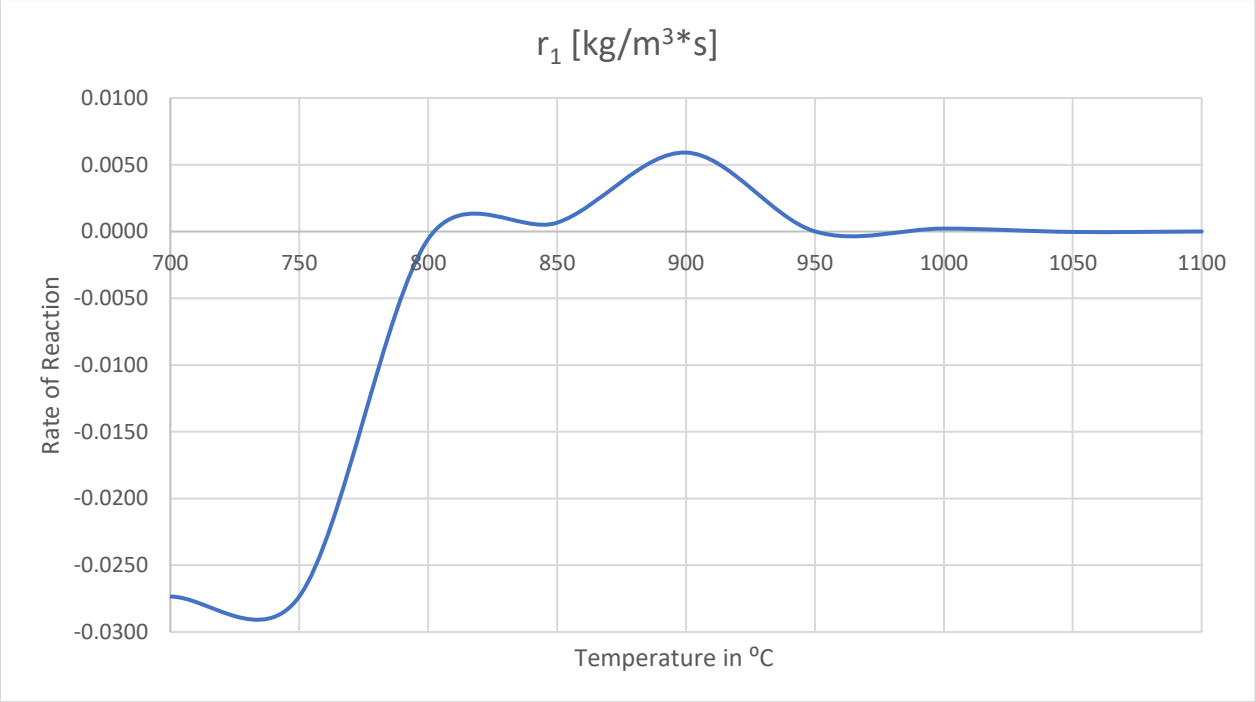

Figure 14: Sensitivity of Temperature on Reaction Rate 1 at Outlet

Reaction rates are shown in Figures *14* and *15*.

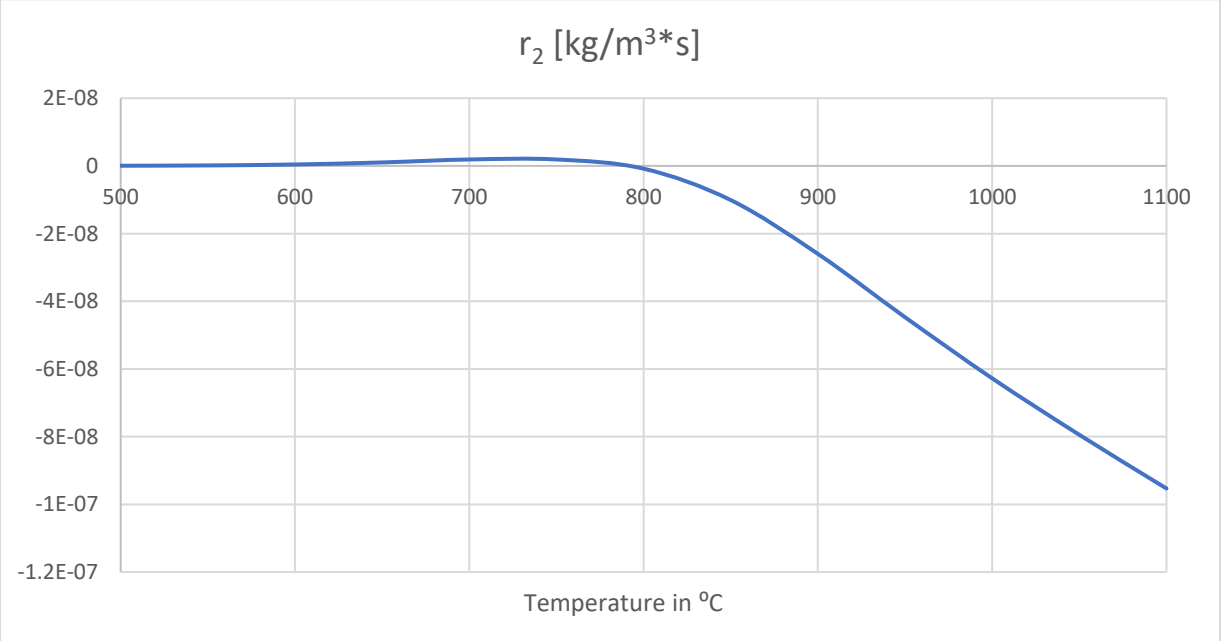

Figure 15: Sensitivity of Temperature on Reaction Rate 2 at Outlet

The rate of r_2 increases slightly with temperature until a critical point is reached at 750°C, then a sharp decrease follows which continues into the negative values. When taking into consideration the exothermic nature of the WGSR, this would imply the highest energy efficiency lies at an operating temperature of around 750°C.

4 FURNACE DESIGN

The heating system of conventional steam reformers used in industry usually involves a large-scale furnace, which features multiple burners fuelled by Natural Gas.

4.1 Mass and Energy Balance

Based on the energy balances obtained in section 3.2, we can calculate the amount of fuel required. As a burner feed raw Natural Gas was selected. *Table 15* shows the composition as well as the heats of combustion for each compound. A total furnace efficiency of 90% was assumed, whereby 50% of energy is transferred to the tubes directly, another 40% gets captured as flue gas (for pre-heating of feed, not calculated within this report) and 10% is lost to the surroundings (Integrated Global Services, 2021).

Table 18: Total Heat of Combustion for Fuel Mixture

Compound	$y3_j$	H_c (kJ/kmol)
CH_4	0.938	-890360
C_2H_6	0.0452	-1559900
C_3H_8	0.0038	-2220000
C_4H_{10}	0.0004	-2878500
C_5H_{12}	0.0002	-3536100
C_6+	0.00029946	-4194800
N_2	0.0073	-
CO_2	0.0047	-
H_2S	5.4464E-07	-562590
Total H_c (mixture)	**1**	**-917305.3**

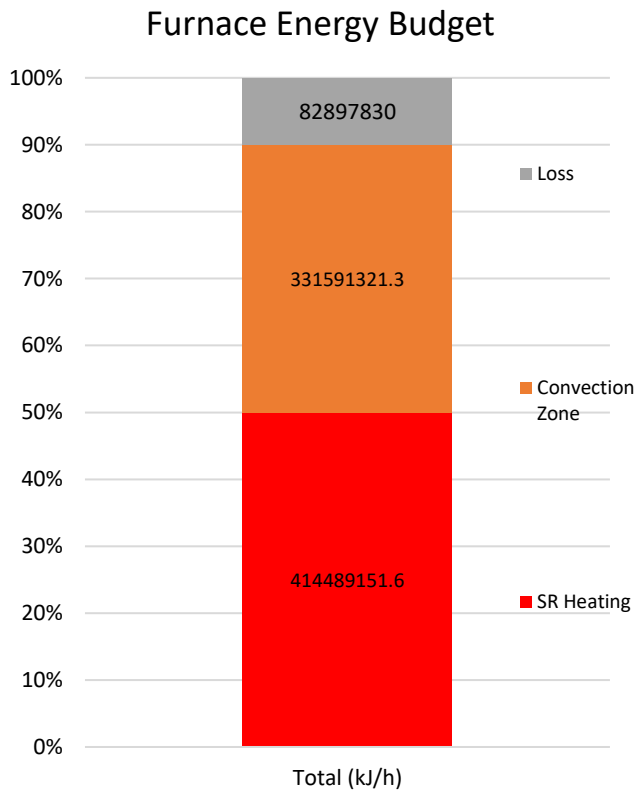

Figure 16: Furnace Energy Budget

The total burner feed required can be calculated as:

$$\frac{Q/H_C}{Efficiency} = \frac{-4.14 * 10^8 \ \frac{kJ}{h} / -917305 \frac{kJ}{kmol}}{0.5} = 903.71 \ kmol/h \qquad \textbf{Equation 26}$$

A diagram was created of the energy budget of the reformer furnace (*Figure 15*).

4.2 Burner Configuration

A variety of SR furnace designs have been developed. The four most commonly used types are listed in *Figure 16*. Configurations C and D were developed by two leading engineering companies in the field, Foster Wheeler and Topsoe. They require a more complex design approach as opposed to configurations A and B; therefore, those designs were discarded as an option for the reformer presented in this report. Configuration A presents a more complex flue gas system (stack must be suspended above SR furnace), therefore configuration B was selected for ease of construction and design. It is commonly used within the available literature on Steam Reformers (Tran, et al., 2017).

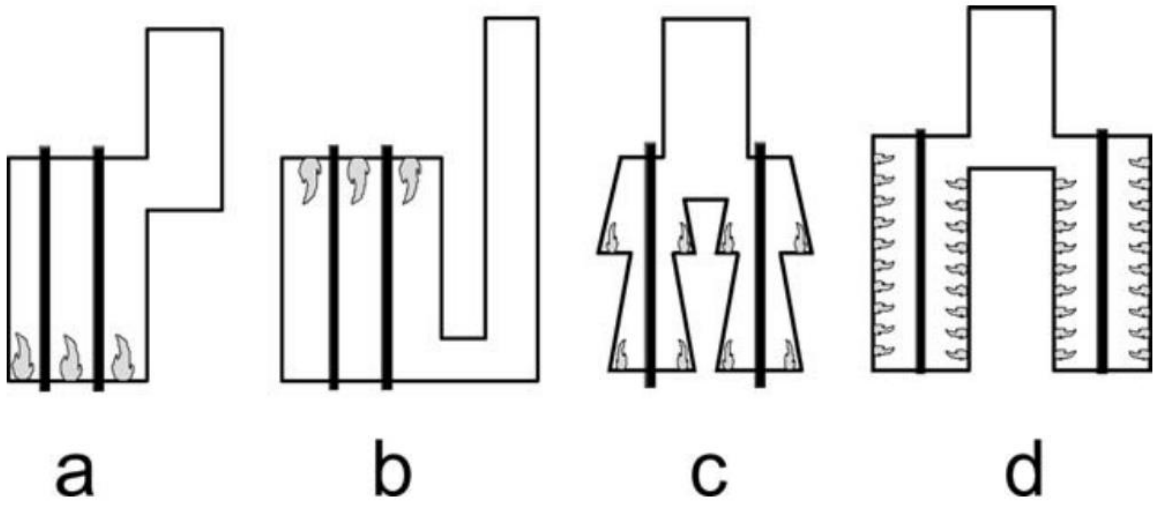

Figure 17: Typical Configurations of Reformer Furnaces: a) Bottom Fired, b) Top Fired, c) Terrace Wall d) Side Fired (Benito & Sanz, 2005)

A total number of 54 burners was selected, giving a tube/burner ratio of ~2.67.

4.3 FURNACE LAYOUT

Some key parameters need to be taken into consideration for the layout of the furnace. These are:

1. Tube Placement
2. Feed Header (pigtail) Placement
3. Burner Placement
4. Flue gas tunnel placement

The tubes were laid out in an arrangement of 3 groups of 8 tubes per row. A total of 8 rows are separated by rows of 6 burners, for a total of 54 burners. This provides a compact design, which is thermally efficient. Feed headers are positioned above, providing co-current flow (burner/tube), which is standard industry practice.

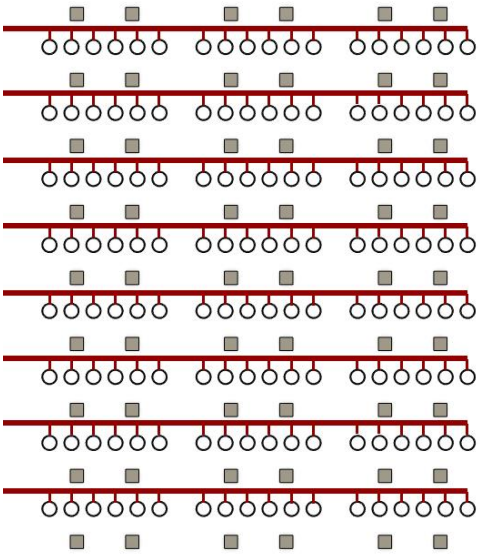

Figure 18: Tube Layout with Manifold and Burner Placement

4.4 Furnace Sizing

Based on the tube layout a total furnace size of 3.7 m by 4.5 m was found to be sufficient. The height of the furnace depends on tube length, so a minimum of 12m.

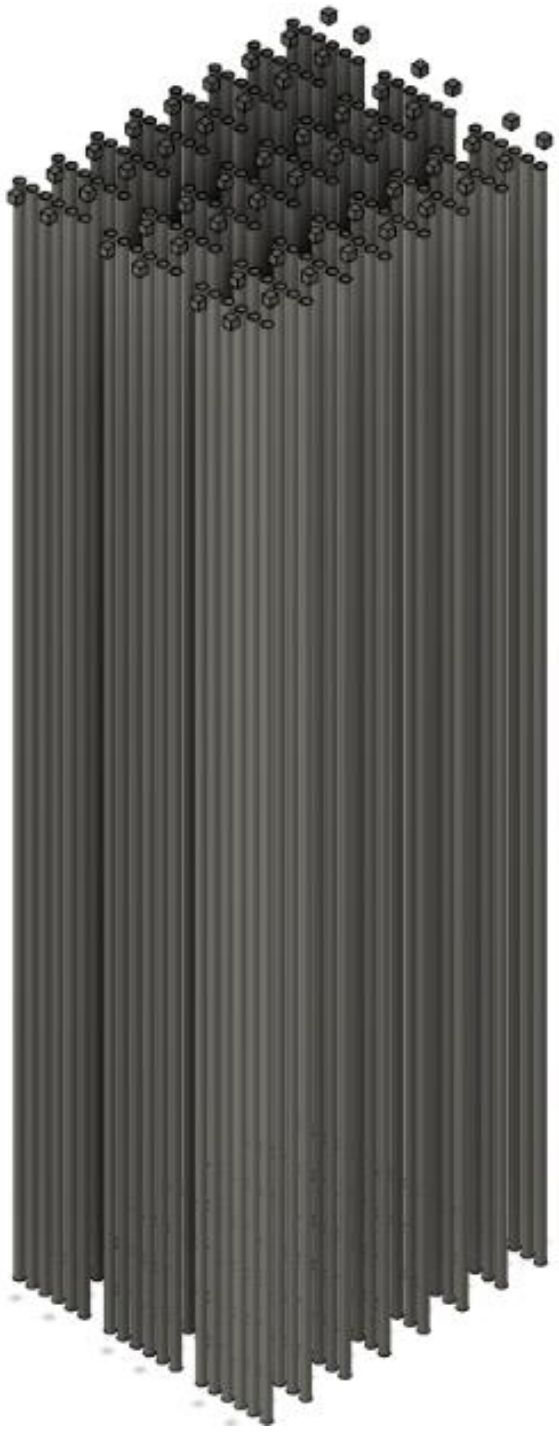

Figure 19: CAD Model of Tube and Burner Layout

5 CONCLUSION

In total, the design of the Steam Reformer was performed successfully. The Mass balances show a H_2 output of 400 t/day, which meets the expected goal. Energy balances give an overall energy consumption of $1.21*10^8$ kJ/h. It also shows the endothermic nature of the overall reaction, which is a critical factor that was considered in the design. An overall volume was derived from the rate equation and design considerations were made. The final volume lies at 54.288 m^3, with an NT of 144. A basic furnace layout was created, considering the tube layout in particular.

Recommended areas of improvement are the effect of the tube material and thickness on heat transfer, convection within the reformer as well as considering the change of pressure through the bed.

REFERENCES

Akers, W. W. & Camp, D. P., 1955. Kinetics of the Methane-Steam Reaction. *AiChE Journal,* 1(4), pp. 471-475.

Benito, M. & Sanz, J. L., 2005. New Trends in Reforming Technologies: from Hydrogen Industrial Plants to Multifuel Microreformers. *Catalysis Reviews,* 47(4), pp. 491-588.

Boudreau, J. & Rocheleau, A., 2010. *Comparison of Catalyst Geometries Using Computational Fluid Dynamics For Methane Steam Reforming,* Worcester: s.n.

Committee on Climate Change, 2019. *Net Zero - The UK's Contribution to Stopping Global Warming.* [Online]
Available at: https://www.theccc.org.uk/wp-content/uploads/2019/05/Net-Zero-The-UKs-contribution-to-stopping-global-warming.pdf

Costamagna, P. et al., 2020. Modeling of Laboratory Steam Methane Reforming and CO2 Methanation Reactors. *Energies,* 13(10), p. 2624.

Dincer, I. & Acar, C., 2015. Review and evaluation of hydrogen production methods for better sustainability. *International Journal of Hydrogen Energy,* 40(34).

Elshout, R., 2010. *Chemical Engineering Online.* [Online]
Available at: https://www.chemengonline.com/hydrogen-production-by-steam-reforming/?printmode=1#:~:text=Steam%2DMethane%20Reforming,-Refinery%20hydrogen%20comes&text=In%20the%20overall%20steam%20methane,monoxide%20and%20some%20carbon%20dioxide.

Felder, R. M. & Rousseau, R. W., 2005. *Elementary Principles of Chemical Processes.* 3rd ed. s.l.:John Wiley & Sons, Inc..

Franchi, G. et al., 2020. Hydrogen Production via Steam Reforming: A Critical Analysis of MR and RMM Technologies. *Membranes,* 10(1), p. 10.

Hawkins, G. B., 2013. *Reduction and Start-Up of Steam Reforming Catalyst,* s.l.: GHB Enterprises, LTD.

Hawkins, G. B., 2013. *Steam Reforming - Poisons,* s.l.: GHB Enterprises LTD..

Hou, K. & Hughes, R., 2001. The kinetics of methane steam reforming over a Ni/α-Al2O catalyst. *Chemical Engineering Journal,* 82(1-3), pp. 311-328.

Hydrocarbon Processing, 2012. *Gas Processes 2012 Handbook.* s.l.:s.n.

Integrated Global Services, 2021. *Primary Reformers.* [Online]
Available at: https://integratedglobal.com/industries/chemical/reformer-efficiency/#:~:text=Thermal%20Efficiency%20of%20the%20Steam,in%20the%20reformer%20convection%20section.
[Accessed 03 May 2021].

Meloni, E., Martino, M. & Palma, V., 2020. A Short Review on Ni Based Catalysts and Related Engineering Issues for Methane Steam Reforming. *Catalysts,* 10(3), p. 352.

NS Energy, 2020. *The five UK hydrogen projects awarded government development funds.* [Online]
Available at: https://www.nsenergybusiness.com/news/hydrogen-production-plants-uk/

Oliveira, E. L. G., Grande, C. A. & Rodrigues, A. E., 2009. Steam Methane Reforming in a Ni/Al2O3Catalyst: Kinetics and Diffusional Limitationsin Extrudates. *The Canadian Journal of Chemical Engineering,* Volume 87, pp. 945-956.

Perry, R. H., Green, R. W. & Maloney, J. O., 1997. *Perry's Chemical Engineer's Handbook.* 7th ed. s.l.:McGraw-Hill.

Pimenidou, P., Rickett, G., Dupont, V. & Twigg, M. V., 2010. High purity H2 by sorption-enhanced chemical looping reforming of waste cooking oil in a packed bed reactor. *Bioresource Technology,* 101(23).

Rashid, K., Dong, S. K. & Mehran, T., 2017. Numerical Investigation for 1kW-Class FT-SOFC System to Evaluate the Compact Size Integrated Hotbox Design. *ECS Transactions,* 78(1), pp. 2569-2579.

Rosetti, V., 2007. *Catalysts for H2 production,* Bologna: Università di Bologna.

Speight, J. G., 2020. The Refinery of the Future (Second Edition). In: s.l.:s.n.

Tran, A. et al., 2017. CFD modeling of a industrial-scale steam methane reforming furnace. *Chemical Engineering Science,* Volume 171, pp. 576-598.

United Nations, 2015. *https://unfccc.int/process-and-meetings/the-paris-agreement/the-paris-agreement.* [Online]
Available at: https://unfccc.int/sites/default/files/english_paris_agreement.pdf

University of Bradford, 2016. *Chemical Engineering Examination Data Book.* 13th ed. Bradford: University of Bradford.

Xu, J. & Froment, G. F., 1989. Methane Steam Reforming, Methanation and Water-Gas Shift: I. Intrinsic Kinetics.. *AiChE Journal,* Volume 35, pp. 88-96.